Parametric Modeling and Simulation of a Simplified Horizontal Tail Under the Framework of Isogeometric Analysis

Xiaoxiao Du[1] [ID], Gang Zhao[2], Wei Wang[3], Yazui Liu[4], Pengfei Zhang[5], Pengfei Han[6] and He Cheng[7]

[1]Beihang University, duxiaoxiao@buaa.edu.cn
[2]Tsinghua University, gangzhao@tsinghua.edu.cn
[3]Beihang University, jrrt@buaa.edu.cn
[4]Beihang University, liuyazui@buaa.edu.cn
[5]Beihang University, ftd423@buaa.edu.cn
[6]Beihang University, hanpf@buaa.edu.cn
[7]Beihang University, naler@buaa.edu.cn

Corresponding author: Gang Zhao, gangzhao@tsinghua.edu.cn

Abstract. In this paper, a parametric design-to-analysis framework is developed for horizontal tail structures, which are constituted of ribs, spars and skins. Given the necessary dimensional parameters and the number of ribs, the horizontal tail structure can be generated automatically by using multiple NURBS patches. To avoid dealing with coupling problems between different patches, the NURBS patches of the generated structure are constrained to conforming along the interfaces. The Reissner-Mindlin isogeometric shell formulations are utilized to solve the static bending and free vibration analysis of the tail structures. The obtained results are compared with those of the commercial software ABAQUS to verify the accuracy and robustness of the proposed method. We also study the influence of the number of ribs on the deformation of the tail.

1 INTRODUCTION

The tail structures, also called stabilizers, in the conventional aircraft configuration are normally arranged at the rear of the fuselage, providing for trim, stability and control [18,20]. It primarily consists of the horizontal tail and the vertical tail as shown in Figure 1. The horizontal tail looks like a little wing and is utilized to balance the aircraft by creating a lift force, which is significant to the safety of an aircraft. A horizontal tail structure generally includes ribs, spars, skins and stringers which are assembled with mechanical fasteners.

The design of horizontal tail structures has always been an interesting topic in the aerospace field [1] and simulation techniques like finite element methods are generally indispensable in the

design process. It is well-known that designed models in CAD systems should be converted into analysis models in CAE systems for simulation and the conversion process is laborious and time-consuming. Isogeometric analysis (IGA) aims to integrate the CAD and CAE models by employing the spline basis functions used for modeling as the shape functions used for simulation [4,12]. This novel concept has attracted great attention in recent years.
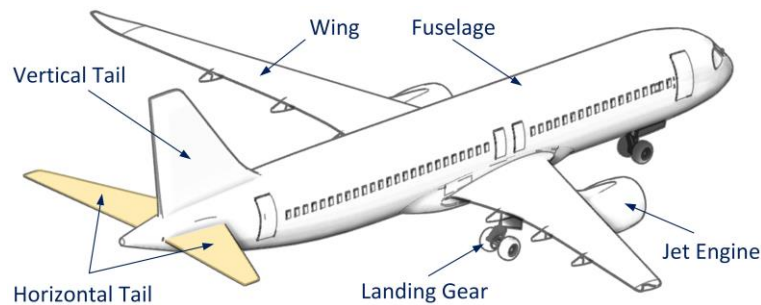
Figure 1: A conventional aircraft configuration and the definitions of the main parts.

NURBS is the dominant technique in geometric modeling and thus is widely used in IGA. Due to the rectangular topological structure of NURBS, a large number of NURBS patches might be used when representing a complicated model. As a consequence, extra work is inevitable to handle patch coupling problems [3,6,7]. It should be pointed out that some other spline functions have been developed, like T-splines [21], unstructured T-splines [22], LR-splines [13], THB-splines [10], to bypass the limitations of NURBS in local refinement and representing complex geometry using a singular patch. However, these novel splines have not been widely applied in CAD systems. In this paper the tail structure is constructed by using multiple conforming NURBS patches, which means the adjacent patches share the same interfacial curves. Such a layout will help us avoid dealing with intricate coupling problems and improve the robustness of the simulation.

The parts of a tail structure are usually designed to be thin in the thickness direction to reduce weight. These structures could be analyzed by using shell theory in simulation to improve computational efficiency. The Reissner-Mindlin and Kirchhoff-Love shell theories are two popular assumptions. The former requires C0 continuity between elements and it is more suitable for moderate and thick shells [2]. The latter requires C1 continuity between elements and is suitable for thin shells [14]. The requirement of C1 continuity across element boundaries is hard to be satisfied in conventional FEA. Even though high continuity in IGA is relatively easy to be satisfied, some extra work should be completed to handle C0 continuities between patches for the Kirchhoff-Love shell theory [11,16].

In this paper, we develop a unified framework for designing and analyzing simplified horizontal tails based on isogeometric analysis, which is considered to be an advanced numerical method from the perspective of CAD/CAE integration. When some basic parameters are given, a horizontal tail can be modeled automatically. Meanwhile, the number of ribs, spars and their layout could also be regarded as design variables. The designed model can be simulated directly using the isogeometric method under the developed framework. The horizontal tail structures with different numbers of ribs are tested under a specific load to study the influence of ribs on the deformation of the tail.

The paper is organized as follows: Section 2 introduces the geometric shape and dimensions of the horizontal tail structure. A parametric modeling technique using multiple NURBS patches is discussed in Section 3 and a brief derivation of isogeometric Reissner-Mindlin shell formulations is presented in Section 4. Section 5 demonstrates the static bending and free vibration analysis of the designed tail using the isogeometric method. Eventually, a conclusion is drawn in Section 6.

2   HORIZONTAL TAIL GEOMETRY

The geometry parameters of a horizontal tail are preliminarily given as: tail span $b = 12.70$ m, aspect ratio $AR = 4.04$, taper ratio $TR = 0.26$, back-ward quarter chord sweep $\Lambda_{1/4} = 30$, dihedral angle $\theta = 7°$. Assume that the planform of the horizontal tail is linearly tapered as shown in Figure 2, then the tail reference area S_W can be expressed as [15]:

$$S_W = \frac{b^2}{A_R} = \frac{1}{2}\left(C_R + C_T\right) \cdot b \tag{2.1}$$

where the parameters C_R and C_T denote the root chord and tip chord of the horizontal tail, respectively. According to the above equation and predefined parameters, we can easily obtain $C_R = 4.9899$ m and $C_T = 1.2973$ m. Given a reference coordinate system, the relative positions of the root chord and tip chord could be defined by the quarter chord sweep.
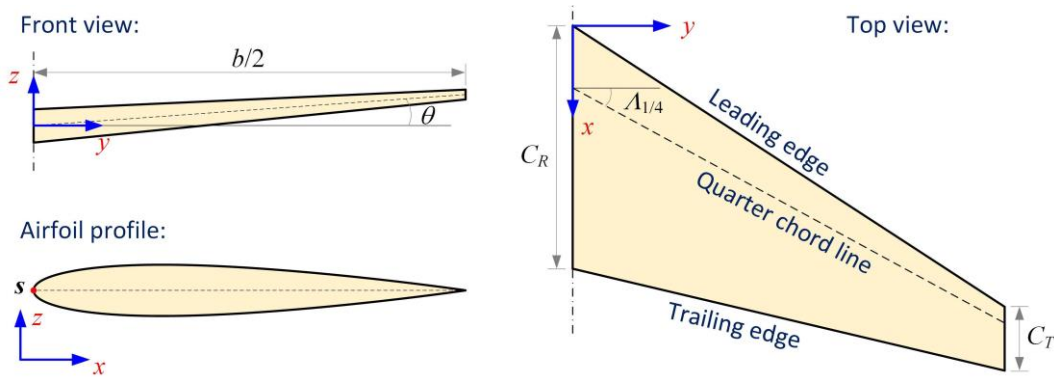
Figure 2: The top view, front view and airfoil profile of a horizontal tail.

As for the airfoil profile of the horizontal tail, we choose the symmetrical NACA-0012 type airfoil, which could be explicitly defined by the formula as [18]:

$$z_t(x) = 0.5 \cdot t \cdot C\left[0.2969\sqrt{\frac{x}{C}} - 0.1260\left(\frac{x}{C}\right) - 0.3516\left(\frac{x}{C}\right)^2 + 0.2843\left(\frac{x}{C}\right)^3 - 0.1015\left(\frac{x}{C}\right)^4\right] \tag{2.2}$$

in which $x \in [0, C]$ and C is the chord length. The calculated z_t indicates the half thickness of the airfoil at the coordinate x. The parameter t denotes the maximum half thickness and is defined by the last two digits in the NACA 4-digits denomination divided by 100. For example, t takes the value 0.12 to the type NACA-0012.

3   PARAMETRIC MODELING

To avoid dealing with trimming and stitching problems in IGA [23], we utilize multiple conforming NURBS patches to build the horizontal tail, which is divided into three parts: ribs, spars and skins. In the following, we will discuss the parametric modeling of these parts in detail.

3.1   Rib Modeling

Ribs are used to provide the shape and thickness of the tail and are spaced along the tail span direction. Assume that the number of ribs is adjustable and only two spars are designed as depicted in Figure 3. Let n_r be the number of ribs and they are equally spaced along the span direction. The first rib and the end rib are located at the root and the tip of the tail. Then the distance between the i-th rib and the aircraft centerline is expressed as

$$d_i = \frac{b}{2(n_r - 1)}i, \quad i = 0, 1, \cdots, n_r - 1. \tag{3.1}$$

For the i-th rib, its chord length C_i could be linearly interpolated from C_R and C_T, written as

$$C_i = C_R - \frac{2(C_R - C_T)}{b} d_i = C_R - \frac{C_R - C_T}{n_r - 1} i. \tag{3.2}$$

When the chord length C_i is obtained, its structural dimensions could be computed with Equation. (3.2). Note that NURBS possesses affine invariance property, we can build NURBS patches for a normalized rib structure and map them to specific positions. The global coordinates of the left endpoint $\mathbf{S}_i$ for the i-th rib, as given in Figure 2, could be expressed as

$$\mathbf{S}_i\left(x, y, z\right) = \left[\frac{1}{4}\left(C_R - C_i\right) + d_i \tan \Lambda_{1/4}, \ d_i, \ d_i \tan \theta\right]. \tag{3.3}$$

Generally, the rib structure is designed with holes to reduce weight. Figure 3 shows an example of the rib structure for the designed horizontal tail. The blue lines denote the spars and the red curve denotes the airfoil profile. Two holes are designed and radius $r = t \cdot C/6$ and $R = t \cdot C/4$.
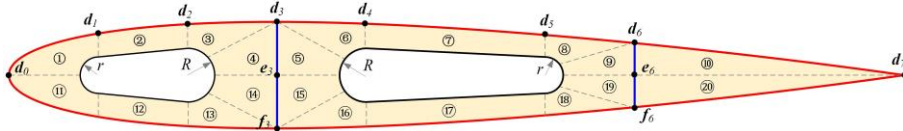
Figure 3: A rib structure of the horizontal tail and its quad-domain segmentation.
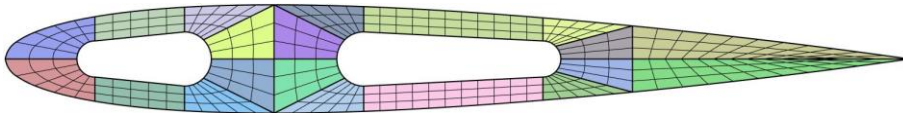
Figure 4: The rib structure is built with 20 conforming NURBS patches.

For multi-patch modeling, the rib structure should be first divided into conforming quad subdomains as depicted in Figure 3, where dotted lines denote the interfaces of subdomains. Each sub-domain is further re-constructed with a single NURBS patch. The airfoil profile is expressed by an explicit function as given in Equation (2.2) and should be re-expressed by a series of NURBS curves. In this paper the LSPIA method [5,17] is used to fit the airfoil profile. According to the domain segmentation, the airfoil profile is divided into seven segments for curve fitting as shown in Fig. 3. The endpoints are labeled as $\mathbf{d}_i$ ($i = 0,1,2, …, 7$).

To construct the patch ①, as labeled in Figure 3, we ought to fit the curve segment $\mathbf{d}_0\mathbf{d}_1$, which is discretized into $m+1$ data points $\mathbf{Q}_j$ ($j=0,1,2, …, m$). Using the classical chord length parameterization method [19], the data point $\mathbf{Q}_j$ is assigned a parameter u_j. Let $n+1$ and $\mathbf{P}_i$ be the number and coordinates of control points, then the fitting curve at the k-th iteration could be generated as

$$C^k(u) = \sum_{i=0}^{n} P_i^k R_i(u). \tag{3.4}$$

At the $(k+1)$-th iteration, the control points are updated by [5]

$$P_i^{k+1} = P_i^k + \Delta_i^k, \quad \Delta_i^k = \mu \sum_{j=0}^{m} R_i(u_j)\delta_j^k, \quad \delta_j^k = Q_j - C^k(u_j), \tag{3.5}$$

in which m is a constant and is recommended to take the value $2/M$ [5]. Let m_i be the sum of the i-th row elements of $\mathbf{A}^T\mathbf{A}$ and $M = \max(m_i)$. $\mathbf{A}$ is a collocation matrix, written as

$$A_{(m+1)\times(n+1)} = \begin{bmatrix} R_0(u_0) & R_1(u_0) & \cdots & R_n(u_0) \\ R_0(u_1) & R_1(u_1) & \cdots & R_n(u_1) \\ \vdots & \vdots & \ddots & \vdots \\ R_0(u_m) & R_1(u_m) & \cdots & R_n(u_m) \end{bmatrix}. \tag{3.6}$$

The iteration process is terminated when the fitting error is lower than the given tolerance. The obtained fitting curve is served as one of the boundary curves of the patch ①. The circular curve segment of the left hole could be exactly represented by a NURBS curve, which is also served as one of the boundary curves. Then the patch ① can be obtained by linearly interpolating these two boundary curves. Similarly, we can construct all the other patches. The final construction of the rib

consists of 20 NURBS patches and is illustrated in Figure 4. Note that the patches ⑩ and ⑳ degenerate at the right shape edge.
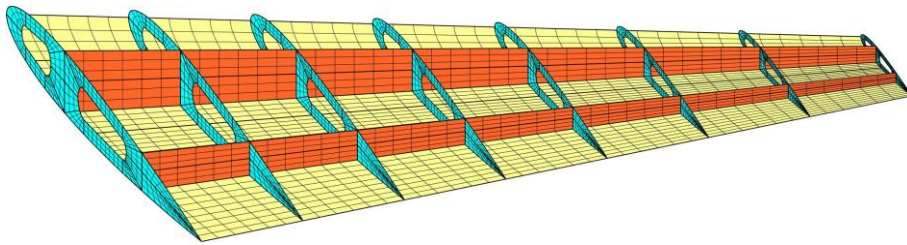
3.2 Spar Modeling

There are two spars designed in the horizontal tail. The blue lines given in Figure 3 are the intersections of spars and ribs, denoted by $\mathbf{d}_3\mathbf{f}_3$ and $\mathbf{d}_6\mathbf{f}_6$. For conforming modeling, each spar between adjacent ribs is constructed with two NURBS patches. The curve segments $\mathbf{d}_3\mathbf{e}_3$ and $\mathbf{e}_3\mathbf{f}_3$ belong to different patches. The coordinates of point $\mathbf{d}_3$ in the local system are represented by $[0.3C, z_t(0.3C)]$. For the i-th rib, the global coordinates of the point $\mathbf{d}_3$ could be represented by

$$\mathbf{d}_3^i = \mathbf{S}_i + [0.3C_i, \quad 0, \quad z_t(0.3C_i)], \tag{3.7}$$

where z_t is calculated by Equation (2.2) and $\mathbf{S}_i$ is given in Equation (3.3). The global coordinates of the points $\mathbf{e}_3$ and $\mathbf{f}_3$ can be easily recovered from $\mathbf{d}_3$. In the same way, point $\mathbf{d}_6$ can be obtained by substituting the coefficient 0.3 given in Equation (3.7) with 0.7. These two position coefficients can also be regarded as design variables.

When the corner points of each spar are calculated, we can construct the intersection lines coincided with the rib structure and linearly interpolate the intersection lines between adjacent ribs. Eventually, two spars are built with $4(n_r-1)$ NURBS patches.

Figure 5: The structural layout of the horizontal tail includes 8 ribs, 2 spars and 2 skins. Each rib is built with 20 NURBS patches. Each spar is built with 14 NURBS patches and each skin is built with 49 NURBS patches.

3.3 Skin Modeling

The skin can be divided into the upper and bottom parts. They can further be modeled by interpolating the adjacent rib profiles. Therefore, there are n_r-1 skin segments and each skin segment is a ruled surface. According to the segmentation of the airfoil profile given in Figure 3, the upper part of the profile is divided into 7 curve segments. As a consequence, the upper skin part between adjacent ribs is constructed by 7 NURBS patches. The whole skin model will include $14(n_r-1)$ NURBS patches.

Figure 5 shows a designed example of the horizontal tail, which consists of 8 ribs, 2 spars and 2 skins. Each rib is built with 20 NURBS patches and is rendered in cyan. Each spar is built with 14 NURBS patches and is rendered in orange. Each skin is built with 49 NURBS patches and is rendered in light yellow. Only the bottom skin part is visualized for better observing the inner structures. There is a total of 286 NURBS patches used for representing the horizontal tail model. For the tail with n_r ribs, the number of NURBS patches should be $38n_r -18$.

4 ISOGEOMETRIC REISSNER-MINDLIN SHELL FORMULATIONS

The Reissner-Mindlin shell theory is utilized to calculate the bending and vibration of tail structures. The shell structure can be represented by its middle surface as [9]

$$\mathbf{x}(\xi, \eta, \zeta) = \bar{\mathbf{x}}(\xi, \eta) + \frac{h}{2}\zeta\mathbf{n}(\xi, \eta), \tag{4.1}$$

in which the parameters (ξ, η) represent the curvilinear coordinates of the middle surface, ζ is the parameters along the thickness direction and h denotes the thickness.

For each control point, there are three translational DOFs (u, v, w) and rotational DOFs $(\theta_x, \theta_y, \theta_z)$. Assume that the simulation is conducted under the situation of linear elasticity and only small deformation is considered. Let R_A be the NURBS function corresponding to the A-th control point, The displacement of the shell can be expressed by

$$u(\xi, \eta, \zeta) = \sum_{A=1}^{n} R_A(\xi, \eta)\left\{\tilde{u}_A + \frac{h}{2}\zeta[\tilde{\theta}_A \times n(\xi, \eta)]\right\}, \tag{4.2}$$

where

$$\tilde{u}_A = \{u^A, v^A, w^A\}^T, \quad \tilde{\theta}_A = \{\theta_x^A, \theta_y^A, \theta_z^A\}^T. \tag{4.3}$$

Let σ and ε be the Voigt form of the stress and strain, written as

$$\sigma = \{\sigma_{xx}, \sigma_{yy}, \sigma_{zz}, \sigma_{xy}, \sigma_{yz}, \sigma_{xz}\}^T, \quad \varepsilon = \{\varepsilon_{xx}, \varepsilon_{yy}, \varepsilon_{zz}, 2\varepsilon_{xy}, 2\varepsilon_{yz}, 2\varepsilon_{xz}\}^T. \tag{4.4}$$

Then the stress-strain relations can be represented by $\sigma = D\varepsilon$ where D is the constitutive matrix, given by

$$D = \frac{E}{1-v^2}\begin{bmatrix} 1 & v & 0 & 0 & 0 & 0 \\ v & 1 & 0 & 0 & 0 & 0 \\ 0 & 0 & 0 & 0 & 0 & 0 \\ 0 & 0 & 0 & \frac{(1-v)}{2} & 0 & 0 \\ 0 & 0 & 0 & 0 & \frac{\kappa(1-v)}{2} & 0 \\ 0 & 0 & 0 & 0 & 0 & \frac{\kappa(1-v)}{2} \end{bmatrix} \tag{4.5}$$

The scalar $\kappa = 5/6$ is the shear correction factor. Considering the discretization of displacement given in Equation (4.2), the strain vector in Equation (4.4) can be rewritten as

$$\varepsilon = \sum_I B_I \tilde{u}_I. \tag{4.6}$$

The sub-matrix B_I is given by

$$B_I = \begin{bmatrix} R_{I,x} & 0 & 0 & 0 & (\bar{R}_I n_3)_x & -(\bar{R}_I n_2)_x \\ 0 & R_{I,y} & 0 & -(\bar{R}_I n_3)_y & 0 & (\bar{R}_I n_1)_y \\ 0 & 0 & R_{I,z} & (\bar{R}_I n_2)_z & -(\bar{R}_I n_1)_z & 0 \\ R_{I,y} & R_{I,x} & 0 & -(\bar{R}_I n_3)_x & (\bar{R}_I n_3)_y & (\bar{R}_I n_1)_x - (\bar{R}_I n_2)_y \\ 0 & R_{I,z} & R_{I,y} & (\bar{R}_I n_2)_y - (\bar{R}_I n_3)_z & -(\bar{R}_I n_1)_y & (\bar{R}_I n_1)_z \\ R_{I,z} & 0 & R_{I,x} & (\bar{R}_I n_2)_x & (\bar{R}_I n_3)_z - (\bar{R}_I n_1)_x & -(\bar{R}_I n_2)_z \end{bmatrix}, \tag{4.7}$$

in which $\bar{R}_I = h\zeta R_I/2$.

Eventually, the equilibrium equations for static bending and free vibration can be expressed as

$$M\ddot{u} + Ku = F, \tag{4.8}$$

where M is the mass matrix, K is the stiffness matrix and F is the external force vector. Discarding the vector, the above equation is used to solve free vibration problems. While discarding acceleration term, the equation is for static bending problems. Generally, the mass matrix and stiffness matrix can be given as

$$M = \int_\Omega R^T mR d\Omega, \quad K = \int_\Omega B^T D_g B d\Omega, \quad m = \rho\begin{bmatrix} h & 0 & 0 \\ 0 & \frac{h^3}{12} & 0 \\ 0 & 0 & \frac{h^3}{12} \end{bmatrix} \tag{4.9}$$

in which ρ is the material density. More details about formulations and implementations of isogeometric Reissner-Mindlin shell can be found in [9].

Note that the rotations about the normal direction are not considered in the conventional Reissner-Mindlin shell theory. Therefore, the stiffness matrix K might suffer from the phenomenon of singularity. A sub-matrix could be added to the specific positions of initial stiffness matrix to avoid the singularity [2],

$$K_A^\theta = K_A^\theta + sk n_A \otimes n_A, \tag{4.10}$$

where K_A^θ denotes the sub-matrix of initial stiffness matrix and n_A is the normal vector related to the A-th control point. The parameter s takes the scalar value with the order of 10^{-4}-10^{-6} [2] and in this work we take 10^{-5}. k is the maximum value of the diagonal components of K_A^θ.

The constructed horizontal tail structure is comprised of multiple NURBS patches. To avoid dealing with non-conforming problems, we constrain the multiple patches to be consistent in the modeling process. For each patch a local sequence of control points is first defined and a global sequence for all control points is then established by renumbering the overlapped control points on the interfaces.

5   NUMERICAL SIMULATION

In this section, we will study the static bending and free vibration analysis of the designed horizontal tail under the framework of isogeometric analysis. The thickness of all the tail structure sections is set as $h = 0.05\text{m}$ and the aluminum alloy 2024-T3 is assigned to each part with Young's modulus of $E = 73.4\text{GPa}$, Poisson's ratio of $\nu = 0.33$, and density of $\rho = 2780 \, \text{kg/m}^3$.
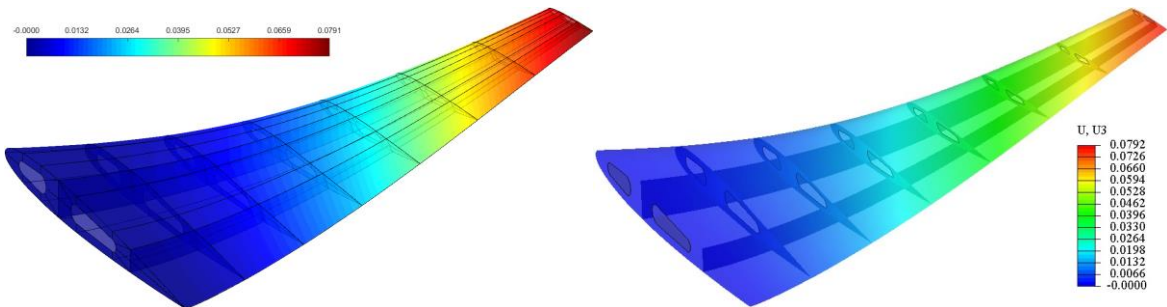
Figure 6: The contour plots of vertical displacement of the horizontal tail obtained by using (a) isogeometric method and (b) finite element method. The deformation scaling factor takes the value 30.
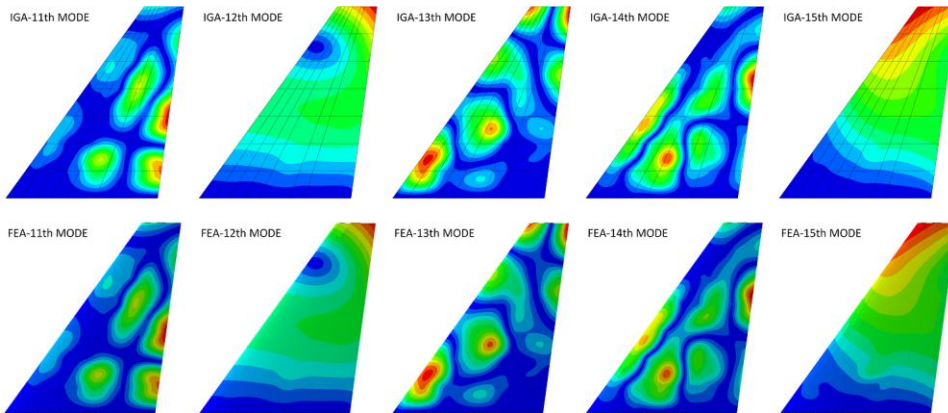
5.1   Static Bending

The upper skin is subjected to a uniformly distributed upward force with the magnitude of $T = 1 \times 10^5 \text{N}$. The end side related to the root chord is fixed. The horizontal tail model includes 8 ribs, 2 spars and 2 skins. The whole model is discretized into 7140 bi-quadratic elements for isogeometric analysis. The contour plot of the obtained vertical displacement is given in Figure 6(a) based on the open-source library NLIGA [8,9]. For comparison, the problem is also solved by using the commercial software Abaqus with 69342 STRI65 elements and the result is shown in Figure 6(b). It can be found that both results agree very well. The maximum vertical displacements obtained by using IGA and FEA are 0.0791m and 0.0792m, respectively.

Methods	Mode 1	Mode 2	Mode 3	Mode 4	Mode 5
IGA	13.480	45.494	59.466	79.320	92.274
FEA	13.474	45.446	59.422	79.300	92.111
Error (%)	0.045	0.106	0.074	0.025	0.177
Methods	Mode 6	Mode 7	Mode 8	Mode 9	Mode 10
IGA	109.17	142.81	155.64	161.33	190.88
FEA	109.01	142.41	155.13	160.97	190.09
Error (%)	0.147	0.281	0.329	0.224	0.416

| Methods	Mode 11	Mode 12	Mode 13	Mode 14	Mode 15
IGA	200.63	204.27	211.30	225.67	233.02
FEA	199.67	204.20	210.50	224.72	232.95
Error (%)	**0.481**	0.034	0.380	0.423	0.030

Table 1: The frequencies of the first 15 modes obtained by IGA and FEA.

Figure 7: The 11th-15th mode shapes of the horizontal tail obtained by the isogeometric method (the upper five sub-figures) and the finite element method (the bottom five sub-figures).

5.2   Free Vibration

Besides the static bending, we also test the free vibration analysis of the horizontal tail. The model is the same as that used for static bending analysis. The end side connected with the root chord is fixed. The first 15th modal vibration behaviors of the tail are studied. Table 1 shows the obtained frequencies $f = \frac{\sqrt{\omega}}{2\pi}$, by using IGA and FEA. The parameter ω is the eigenvalue computed from equation (4.8). It can be observed that both results show good agreement. The relative errors, computed by $Err = (f_{IGA}-f_{FEA})/f_{FEA}$, are also listed. The maximum relative error is 0.481%, which occurred in Mode 11. Additionally, the mode shapes of the 11th to 15th modes are plotted in figure 7, where the color contours present close agreement.
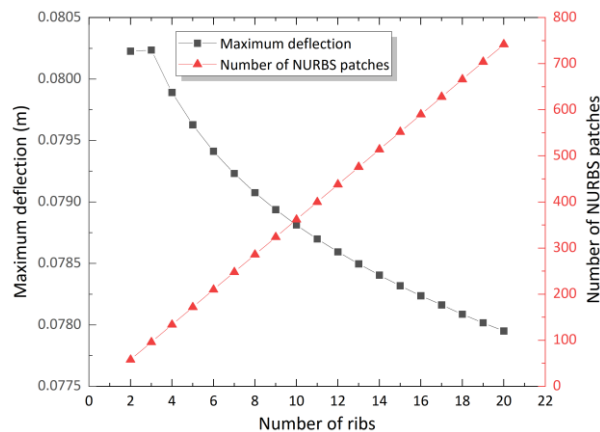
Figure 8: The variations of the maximum deflections and the numbers of NURBS patches for the designed horizontal tail structure with respect to the numbers of ribs.

5.3 Influence of Number of Ribs

Finally, we investigate the influence of the number of ribs on the deflection behaviors of the tail structure. We construct the tail with total np ribs ($np = 2,3,4, ..., 20$) and the ribs are equally spaced along the tail span direction. Note that the number of NURBS patches for the whole tail structure is linear with the number of ribs. Figure 8 shows the variation curve of the maximum deflections with respect to the number of ribs. Except for the tail with 2 ribs, the maximum deflection decreases gradually as expected. The maximum deflections for the tail with 2 and 3 ribs under refined mesh densities are 0.08023m and 0.08024m, respectively. Consequently, it can be argued that adding only one inner rib will not improve the bending resistance of the horizontal tail. When the number of ribs takes the value 20, the number of NURBS patches achieves 742 and the maximum deflection is 0.07795m.

Additionally, the computation times for geometrical modeling, mesh construction, global stiffness computation, rotational stiffness correction and solving equations are listed in Table 2 under the situation of various numbers of ribs. It can be found that the computation of global stiffness takes up most of the time and the average percentage is 90.43%. Different from that mesh generation occupies much time in the traditional finite element method, the geometrical modeling and mesh structure construction only consume 1.31% and 0.50% average percentage of the total time, respectively. We should point out that the current statistics are obtained from our in-house MATLAB codes without further optimization and the procedure is implemented on a laptop with a 2.80 GHz i7-1165 CPU and 16GB RAM. Figure 9 shows the contour of the vertical displacement for the tail structure with 20 ribs obtained by using IGA. The grey framework presents the undeformed boundary curves of NURBS patches.

Number of ribs	Computation time (s) / Percentage (%)				
	Geometrical Modeling	Mesh construction	Global stiffness computation	Rotational stiffness correction	Solving equation
2	0.95 / 3.02	0.26 / 0.82	27.97 / 88.77	1.68 / 5.34	0.65 / 2.05
4	1.57 / 1.66	0.61 / 0.65	83.21 / 87.92	4.59 / 4.85	4.67 / 4.93
6	2.41 / 1.35	0.96 / 0.54	155.08 / 87.21	7.71 / 4.33	11.66 / 6.56
8	5.24 / 1.70	1.85 / 0.60	272.83 / 88.62	14.21 / 4.62	13.74 / 4.46
10	5.03 / 1.21	2.32 / 0.56	377.34 / 91.12	14.64 / 3.53	14.77 / 3.57
12	5.05 / 0.98	2.18 / 0.42	470.10 / 91.67	18.16 / 3.54	17.35 / 3.38
14	5.91 / 0.89	2.51 / 0.38	612.02 / 92.22	22.06 / 3.32	21.17 / 3.19
16	6.86 / 0.84	2.95 / 0.36	760.17 / 92.94	25.73 / 3.15	22.23 / 2.72
18	7.47 / 0.75	3.31 / 0.33	930.07 / 92.82	35.08 / 3.50	26.05 / 2.60
20	8.46 / 0.69	3.73 / 0.30	1115.67 / 91.04	40.74 / 3.32	56.93 / 4.64
Average percentage	1.31	0.50	90.43	3.95	3.81

Table 2: The computation time for modeling and analysis of tail structure with various numbers of ribs.

6 CONCLUSIONS

We developed an isogeometric framework for parametric modeling and simulation of a simplified horizontal tail of airplanes. Given necessary geometric parameters, the tail could be automatically constructed by a series of conforming NURBS patches. Additionally, the tail structure could be adaptively modified according to the number of ribs. The isogeometric Reissner-Mindlin shell is employed to study the static bending and free vibration of the tail and the obtained results are verified by comparing them with FEA results. The maximum deflection of the tail structures will

decrease gradually with the increase in the number of ribs. Therefore, the stiffness of the tail could be improved by increasing the number of ribs. The proposed method is believed to be accurate and robust through the comparisons of the results with that from commercial software and the series of tests with different numbers of ribs.
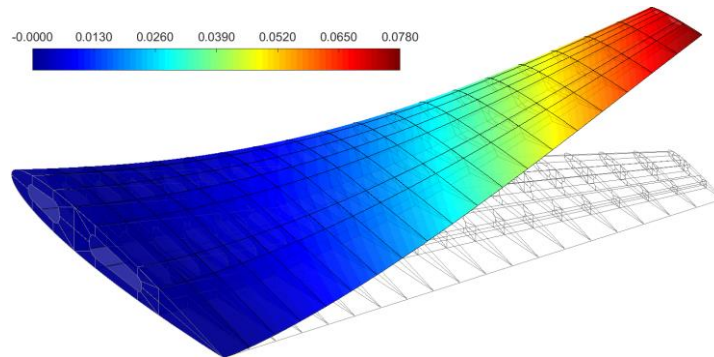
Figure 9: The contour plots of vertical displacement of the horizontal tail with 20 ribs obtained by using isogeometric method.

7 ACKNOWLEDGMENTS

Xiaoxiao Du, http://orcid.org/0000-0002-2324-1005

REFERENCES

[1]   Altunkaya, E.C.; Ozkol, I.: Multi-parameter aerodynamic design of a horizontal tail using an optimization approach, Aerospace Science and Technology, 121, 2022, 107310. https://doi.org/10.1016/j.ast.2021.107310
[2]   Benson, D. J.; Bazilevs, Y.; Hsu, M. C.; Hughes, T.J.R.: Isogeometric shell analysis: the Reissner-Mindlin shell, Computer Methods in Applied Mechanics and Engineering, 199(5-8), 2010, 276-289. https://doi.org/10.1016/j.cma.2009.05.011
[3]   Coox, L.; Greco, F.; Atak, O.; Vandepitte, D.; Desmet, W.: A robust patch coupling method for NURBS-based isogeometric analysis of non-conforming multipatch surfaces, Computer Methods in Applied Mechanics and Engineering, 316, 2017, 235-260. https://doi.org/10.1016/j.cma.2016.06.022
[4]   Cottrell, J.A.; Hughes, T.J.; Bazilevs, Y.: Isogeometric analysis: toward integration of CAD and FEA, John Wiley & Sons, 2009.
[5]   Deng, C.; Lin, H.: Progressive and iterative approximation for least squares B-spline curve and surface fitting, Computer-Aided Design, 47, 2014, 32-44. http://doi.org/10.1016/j.cad.2013.08.012
[6]   Du, X.; Zhao, G.; Wang, W.: Nitsche method for isogeometric analysis of Reissner-Mindlin plate with non-conforming multi-patches, Computer Aided Geometric Design, 35, 2015, 121-136. https://doi.org/10.1016/j.cagd.2015.03.005

[7]   Du, X.; Zhao, G.; Wang, W.; Fang, H.: Nitsche's method for non-conforming multipatch coupling in hyperelastic isogeometric analysis, Computational Mechanics, 65(3), 2020, 687-710. https://doi.org/10.1007/s00466-019-01789-x

[8]   Du, X.; Zhao, G.; Wang, W.; Guo, M.; Zhang, R.; Yang, J.: NLIGA: A MATLAB framework for nonlinear isogeometric analysis, Computer Aided Geometric Design, 80, 2020, 101869. https://doi.org/10.1016/j.cagd.2020.101869

[9]   Du, X.; Zhao, G.; Zhang, R.; Wang, W.; Yang, J.: Numerical implementation for isogeometric analysis of thin-walled structures based on a Bézier extraction framework: nligaStruct, Thin-Walled Structures, 180, 2022, 109844. https://doi.org/10.1016/j.tws.2022.109844

[10]   Giannelli, C.; Jüttler, B.; Speleers, H.: THB-splines: The truncated basis for hierarchical splines, Computer Aided Geometric Design, 29(7), 2012, 485-498. https://doi.org/10.1016/j.cagd.2012.03.025

[11]   Herrema, A.J.; Johnson, E.L.; Proserpio, D.; Wu, M.C.; Kiendl, J.; Hsu, M.C.: Penalty coupling of non-matching isogeometric Kirchhoff – Love shell patches with application to composite wind turbine blades, Computer Methods in Applied Mechanics and Engineering, 346, 2019, 810-840. https://doi.org/10.1016/j.cma.2018.08.038

[12]   Hughes, T. J.; Cottrell, J. A.; Bazilevs, Y.: Isogeometric analysis: CAD, finite elements, NURBS, exact geometry and mesh refinement, Computer methods in applied mechanics and engineering, 194(39-41), 2005, 4135-4195. https://doi.org/10.1016/j.cma.2004.10.008

[13]   Johannessen, K.A.; Kvamsdal, T.; Dokken, T.: Isogeometric analysis using LR B-splines, Computer Methods in Applied Mechanics and Engineering, 269, 2014, 471-514. https://doi.org/10.1016/j.cma.2013.09.014

[14]   Kiendl, J.; Bletzinger, K.-U.; Linhard, J.; Wüchner, R.: Isogeometric shell analysis with Kirchhoff-Love elements, Computer Methods in Applied Mechanics and Engineering, 198, 2009, 3902-3914. https://doi.org/10.1016/j.cma.2009.08.013

[15]   Kundu, A. K., Price, M. A., & Riordan, D.: Conceptual Aircraft Design: An Industrial Approach, John Wiley & Sons, Hoboken, NJ, 2019.

[16]   Leonetti, L.; Liguori, F.S.; Magisano, D.; Kiendl, J.; Reali, A.; Garcea, G.: A robust penalty coupling of non-matching isogeometric Kirchhoff-Love shell patches in large deformations, Computer Methods in Applied Mechanics and Engineering, 371, 2020, 113289. https://doi.org/10.1016/j.cma.2020.113289

[17]   Lin, H.; Maekawa, T.; Deng, C.: Survey on geometric iterative methods and their applications, Computer-Aided Design, 95, 2018, 40-51. https://doi.org/10.1016/j.cad.2017.10.002

[18]   Moran, J.: An introduction to theoretical and computational aerodynamics, John Wiley & Sons, New York, NY, 2003.

[19]   Piegl, L.; Tiller, W.: The NURBS book, 2nd ed, Springer-Verlag, New York, NY, 1997. https://doi.org/10.1007/978-3-642-59223-2

[20]   Raymer, D.P.: Aircraft design: a conceptual approach, 6th ed, American Institute of Aeronautics and Astronautics, Inc., Reston, VA, 2018.

[21]   Sederberg, T.W.; Zheng, J.; Bakenov, A.; Nasri, A.: T-splines and T-NURCCs, ACM Transactions on Graphics, 22(3), 2003, 477-484. https://doi.org/10.1145/882262.882295

[22]   Yang, J.; Zhao, G.; Wang, W.; Du, X.; Zuo, C.: Non-uniform C1 patches around extraordinary points with applications to analysis-suitable unstructured T-splines, Computer Methods in Applied Mechanics and Engineering, 405, 2023, 115849. https://doi.org/10.1016/j.cma.2022.115849

[23]   Zhao, G.; Du, X.; Wang, W.; Liu, B.; Fang, H.: Application of isogeometric method to free vibration of Reissner–Mindlin plates with non-conforming multi-patch, Computer-Aided Design, 82, 2017, 127-139. https://doi.org/10.1016/j.cad.2016.04.006